Microscopic model analyses of elastic proton-^{12}C scattering with energies 40 to 800 MeV

P. K. Deb and K. Amos
School of Physics, University of Melbourne, Victoria 3010, Australia
(Received 29 November 1999; published 19 July 2000)

Medium modified effective two nucleon interactions have been defined for protons incident upon ^{12}C with energies ranging from 40 to 800 MeV. Those effective interactions have been folded with ground state density matrices from a large space shell model of ^{12}C to give complex nonlocal optical potentials. With those the elastic scattering differential cross sections and analyzing powers have been analyzed. Good results are obtained when the effective interactions are linked to *NN* interactions that fit *NN* scattering data and when exchange amplitudes in scattering that lead to strong nonlocality in the optical potentials are taken into account.

PACS number(s): 25.40.Cm, 24.10.Ht, 21.30.Fe, 24.70.+s

I. INTRODUCTION

Elastic scattering, the predominant event associated with the interactions of nucleons with nuclei, has been studied extensively over many decades. From experiment there now exists a vast database. Extensive theoretical studies of such scattering also have been made and based upon inverse scattering theory, of global [1] and of numerical inversion form [2], as well as upon direct scattering theory. In the latter, optical potentials are specified in terms of underlying two-nucleon (*NN*) interactions. Those direct scattering theory optical potentials have been formulated in momentum space [3] and also in coordinate space [4–6].

Herein we investigate facets of the coordinate space formulation of optical potentials, primarily concerned with what *NN* interaction characteristics are required to specify appropriate optical potentials and what effect the attendant nonlocality of those potentials have. An appropriate optical potential we take as one with which successful predictions of nucleon-nucleus (*NA*) elastic scattering data over a large range of energy may be obtained. To this end, complex, nonlocal optical potentials have been obtained by folding effective two-nucleon (*NN*) interactions with a ground state wave function from a large space shell model structure of the nucleus. The effective interactions have been derived from complex *NN* interactions which fit (complex) *NN* scattering phase shifts to over 800 MeV with application to proton-^{12}C scattering in mind.

With this approach and at energies of 65 and 200 MeV, successful predictions of observables from elastic proton-nucleus (*pA*) scattering from many nuclei have been made [5]. But to do so, the inhomogeneous partial wave Schrödinger equations specified by the complex, nonlocal and energy-dependent optical potentials had to be solved without any localization approximation. Medium effects of Pauli blocking and of the average fields in which the projectile and struck nucleon propagate had to be taken into account in specification of the effective *NN* interactions also. This process thus is defined hereafter as *g* folding.

To make predictions of *NA* scattering under the basic assumption that the scattering is due essentially to just pairwise interactions between the projectile and each and every nucleon in the target, three basic aspects of the system under investigation must be specified. Where possible with this approach, such should be defined independently of the *NA* scattering system being studied. First, the description of the nucleus, and in particular the one body density matrix elements (OBDME), should be determined from a large scale structure calculation which describes well the ground state properties of the nucleus in question. This information in combination with the second ingredient, the single particle (bound state) wave functions, can be assessed further by the level of agreement their use gives in predicting elastic electron scattering form factors. Since these wave functions are energy independent, they should not be varied in further application such as seeking better reproduction of specific sets of *NA* scattering data. The final ingredient is a complex, energy and density dependent, effective *NN* interaction that describes the interaction between the incident nucleon and each and every struck nucleon.

For incident energies to 800 MeV, elastic scattering may be described by optical potentials though it has been suggested [7] that they should be formed by folding relativistic density dependent effective interactions (Lorentz invariant amplitudes) with relativistic nuclear structure wave functions. However, based upon the success of using *g* folding (nonrelativistic scattering) optical potentials to analyze elastic scattering of 65 and 200 MeV protons from targets ranging ^{3}He to ^{238}U [5], we consider herein just what may be achieved to 800 MeV with that approach and allowing minimal relativity by using relativistic kinematics. Our interest is in what net effects arise when one uses an effective interaction that is linked to a good description of the *NN* scattering phase shifts. With this aim it is important to note that we make predictions to compare with the scattering data. All details entering the folding process were set *a priori* and single calculations made to specify the differential cross sections and analyzing powers.

In Sec. II we present a brief outline of the microscopic optical potential and its specification in terms of the effective interactions that are folded with OBDME from a large space shell model calculation of the nuclear structure. Details of that structure and of the effective interaction properties are given. The results of proton-^{12}C elastic scattering calculations obtained with those optical potentials are then compared with data in Sec. III. Such comparisons (of differential

cross sections and analyzing powers) are made with data taken at 18 energies in the range 40 to 800 MeV. Specifically we consider the data taken at 40 [8], 50 [9], 65 [10], 120 [11], 135 [12,13], 144 [14], 156 [15], 160 [16], 185 [17], 200 [18], 250 [19], 300 [20,21], 318 [22], 398, 597, and 698 [23], 500 [24], and at 800 MeV [25]. Conclusions are drawn in Sec. IV.

II. THE MICROSCOPIC OPTICAL POTENTIAL

As a detailed presentation of the coordinate space microscopic optical potential has been published [4–6], only salient features of that development are given herein. We presume that *NA* elastic scattering for all the energies of interest can be described in terms of the phase shifts extracted from the asymptotic behavior of solutions of Schrödinger equations

$$\left[\frac{\hbar^2}{2\mu}\nabla^2 - V_c(r) + E\right]\Psi(\mathbf{r}) = \int U(\mathbf{r},\mathbf{r}';E)\Psi(\mathbf{r}')d\mathbf{r}', \quad (1)$$

where, with $\mathbf{r},\mathbf{r}'$ being relative *NA* coordinates, $V_c(r)$ is a Coulomb interaction and $U(\mathbf{r},\mathbf{r}')$ is the optical potential which may be nonlocal, complex, and energy dependent. Relativistic kinematics have been used to ascertain the wave numbers and momentum transfers. Partial wave expansions give the Schrödinger equations as

$$\left[\frac{\hbar^2}{2\mu}\left\{\frac{d^2}{dr^2} - \frac{l(l+1)}{r^2}\right\} - V_c(r) + E\right]\chi_l(k,r) = \int_0^\infty w_l(r,r')\chi_l(k,r')dr'. \quad (2)$$

For simplicity all aspects involving intrinsic spin have been suppressed. Solutions of Eqs. (2) have been evaluated for all of the cases studied using the program DWBA98 [26] with scattering phase shifts and amplitudes extracted and used to specify cross sections, analyzing powers, and for energies 65 and 500 MeV other spin observables, for proton-^{12}C scattering. That computer program does not evaluate the multipoles of the nonlocal microscopic optical potential explicitly. Rather, and using two helicity formalisms, particle-hole matrix elements of a chosen energy and density dependent effective interaction are generated and used in solution of the integrodifferential equations. Nevertheless, development of the form of the optical potential is useful for later discussion. Essentially those potentials result from the overlap functions

$$U_{NA}(1,1') = \left\langle \Psi_{gs}(1',2',\ldots,A') \left| \sum_{n=1}^{A} g(n0) \right| \Psi_{gs}(1,2,\ldots,A) \right\rangle, \quad (3)$$

where the incident projectile is linked to the coordinates ''0'' and $g(n0)$ is the effective interaction that is assumed to be a pairwise entity between that projectile and the nth bound nucleon in the target.

A cofactor expansion the nuclear states

$$|\Phi_{JM}(1,2,\ldots,A)\rangle = \frac{1}{\sqrt{A}}\sum_\alpha a_\alpha |\Phi_{JM}(1,2,\ldots,A)\rangle |\phi_\alpha(1)\rangle, \quad (4)$$

where $\alpha=\{(nl)jm\}$, permits a factorization of the many-nucleon matrix elements so that for the case $J=0$,

$$U_{pA} = \sum_{\alpha\alpha'} \langle \Psi_{gs}^{J=0}|a_{\alpha'}^\dagger a_\alpha|\Psi_{gs}^{J=0}\rangle \langle \phi_{\alpha'}(1')|g_{10}|\phi_\alpha(1)\rangle = \sum_{\alpha\alpha'} \frac{1}{\sqrt{2j+1}} \langle \Psi_{gs}^{J=0}||[a_{\alpha'}^\dagger \times \tilde{a}_\alpha]^{(0)}||\Psi_{gs}^{J=0}\rangle \times \langle \phi_{\alpha'}(1')|g_{10}|\phi_\alpha(1)\rangle \quad (5)$$

on using the Wigner-Eckart theorem. Therein $\langle \Psi_{gs}^{J=0}||[a_{\alpha'}^\dagger \times a_\alpha]^{(0)}||\Psi_{gs}^{J=0}\rangle$ are OBDME. In general for a ground state expectation those OBDME are defined by

$$S_{\alpha\alpha' I}^{J_{gs}} = \langle \Psi_{gs}^J||[a_{\alpha'}^\dagger \times \tilde{a}_\alpha]^{(I)}||\Psi_{gs}^J\rangle, \quad (6)$$

and are obtained directly from the shell model wave functions. However for ^{12}C as $J_{gs}=I=0$, the OBDME are expressed simply by

$$\sigma_{\alpha\alpha'} = \frac{1}{2j+1} S_{\alpha\alpha' 0}^0. \quad (7)$$

For $\alpha=\alpha'$, these are fractional shell occupancies of nucleons.

Thus the microscopic optical potential takes the form

$$U(\mathbf{r},\mathbf{r}';E) = \sum_{\alpha,\alpha'} \sqrt{(2j+1)}\sigma_{\alpha\alpha'}\Big[\delta(\mathbf{r_1}-\mathbf{r_2}) \times \int \phi_{\alpha'}^*(\mathbf{s})U^{(D)}(r_{1s})\phi_\alpha(\mathbf{s})d\mathbf{s} + \phi_{\alpha'}(\mathbf{r_1})U^{(Ex)}(r_{12})\phi_\alpha(\mathbf{r_2})\Big], \quad (8)$$

where $r_{12}=|\mathbf{r_1}-\mathbf{r_2}|$ and $U^{(D)}$ and $U^{(Ex)}$ are combinations of the multipoles of the effective *NN* interactions as one deals with the direct and exchange elements of the folding process. More details are given in Refs. [6,27].

A. The structure information for ^{12}C

With most studies needing the nucleon based properties of ^{12}C, $0p$-, or at best $0p1s0d$-shell model calculations [28] of the structure have been used, although they are known to be limited. Such models predict a spectrum with which large effective charges are needed to map measured electromagnetic transition rates. That is not the case now with current larger space calculations of structure. With a full $(0+2)\hbar\omega$ model space, the positive parity states of ^{12}C have been specified while the negative parity spectrum was found

also but by using a $(1+3)\hbar\omega$ model space [4]. All known states to 20 MeV excitation were matched by candidates from this structure model and to within 2 MeV. Indeed use of this spectroscopy in an analysis [29] of 200 and 398 MeV proton inelastic scattering cross sections and analyzing powers permitted an identification of J^{π}; T values for states in ^{12}C that hitherto had uncertain assignments. As a complete basis was used [for the $(0+2)\hbar\omega$ case at least] there is no spurious center of mass facet in the state specifications. We have used the ground state wave function of that large space shell model in this study.

In forming the optical potentials, besides the OBDME one needs single nucleon bound state wave functions. Frequently they have been chosen as harmonic oscillator (HO) wave functions, but and as seen previously [4] for ^{12}C specifically, a more realistic representation is to use Woods-Saxon (WS) bound state wave functions. With the OBDME determined from the $(0+2)\hbar\omega$ shell model wave functions and the single nucleon bound states appropriately specified, electron scattering form factors from both the elastic and inelastic scattering of electrons from ^{12}C were well fit [4].

B. The effective *NN* interactions

The effective interaction between two nucleons, one the projectile and the other a bound particle in the nucleus, is required in coordinate space and as a combination of central, tensor and two-body spin-orbit terms. Each term can have a linear combination of Yukawa functions as its form factor, and the (complex) strengths of those Yukawa functions may vary with the density of the nuclear medium. These effective interactions have been defined by optimally mapping [30] to half-off-shell (momentum space) *NN* *g*-matrix elements determined from solutions of the Brueckner-Bethe-Goldstone (BBG) equations.

We consider a realistic microscopic model of *pA* reactions to be one that is based upon *NN* interactions whose on-shell values of *t* matrices (solutions of the Lippmann-Schwinger equations) are consistent with measured *NN* scattering data to and above the incident energies of interest. Below pion threshold, the phenomenology of the *NN* interaction is relatively simple, and several one boson exchange potential (OBEP) models [31,32] exist with which very good fits have been found to *NN* phase shift data. Above pion threshold, that is no longer the case. Inelastic channels open and resonance scattering occurs. Simple potentials must be varied to account for the various meson production thresholds and also to account for effects of known [$P_{33}(1232)$ (Δ) and $P_{11}(1440)$ (N^*)] resonance structures in the *NN* system. There exist extensions to OBEP models which incorporate resonance [31] and particle production [33], and with which some *NN* and $NN\pi$ data up to 1 GeV may be explained. The *NN* phase shifts above pion threshold found with these models are better than any from standard OBEP but as yet they are not adequate in a number of important channels. However, the characteristics of the experimental *NN* scattering amplitudes to 2.5 GeV are consistent with an (*NN*) optical potential concept. Recently [34] the SM97 data [35] has been interpreted very well by a basic OBEP supplemented by sensible complex optical potentials. With the OBEP component established by the fits its use gave with data below 300 MeV, the supplementing *NN* optical potentials reflected the effects of the $P_{33}(1232)$ and $P_{11}(1440)$ resonances in several partial waves. Otherwise the optical potentials are smooth, complex, energy dependent, and short ranged which is consistent with the view of production processes being localized at and within the confinement surface of a nucleon. Those *NN* optical potentials also are consistent with the geometry of the profile function as it is known from analyses of high-energy diffraction scattering. We have used the optical potential approach [34] for the *NN* interaction for energies 300 to 800 MeV to define the effective interactions required in the *g*-folding process to give *NA* optical potentials. Specifically we have considered the coupled channel Bonn (BCC3) interaction [31] supplemented with complex, short ranged Gaussian potentials [34]. Those Gaussians were parametrized so that the *t* matrices of the modified BCC3 force on the energy shell match precisely the SM97 data sets. We have also used the one solitary boson exchange potential (OSBEP) [32] as the bare *NN* starting interaction.

This simple model prescription encompasses a plethora of terms that will be needed to adapt a more fundamental boson exchange model approach to adequately explain the *NN* scattering data to 1 GeV and higher. Not only do such boson model calculations increase in complexity with energy but also the number of adjustable parameters involved increase with every additional element incorporated in the theory, making the approach a less appealing way to treat *NN* scattering. Nevertheless it is a goal worth seeking and if, in the fullness of time, such a boson exchange model prescription can be found that meets the requirement that the empirical *NN* *t* matrices are reproduced then we will adapt our studies. But such is not the case at present.

Nevertheless, use of an extending complex potential to adapt standard (below threshold) *NN* prescriptions so that the free *NN* scattering data to over 1 GeV are reproduced means that any specific effect of the Δ and N^* in specification of the *NN* *g* matrices will not be treated. Medium effects upon the Δ propagation could differ from those we set with the complex potential factors defining our effective *g* matrices. However, Ray [36] has studied the effects of including Δ and N^* Pauli blocking in a momentum space formulation of *NN* and *NA* scattering. He concludes that such variation results in only small changes in density-dependent amplitudes at central nuclear densities ($\sim$1.4 fm^{-1}). Ray states specifically ''The lack of sensitivity to Δ blocking supports the Paris-Hamburg effective interaction model which does not treat virtual Δ propagation explicitly.'' As our force is an upgraded version of the Paris-Hamburg model we therefore take heart from that observation of Ray. It is worthwhile noting also that Ray observed that predicted *NA* elastic scattering observables were not very sensitive to the poorly known isobar-nucleus interaction potentials.

III. RESULTS OF CALCULATIONS

Medium modified, complex, effective interactions determined in the manner described have been used to define the

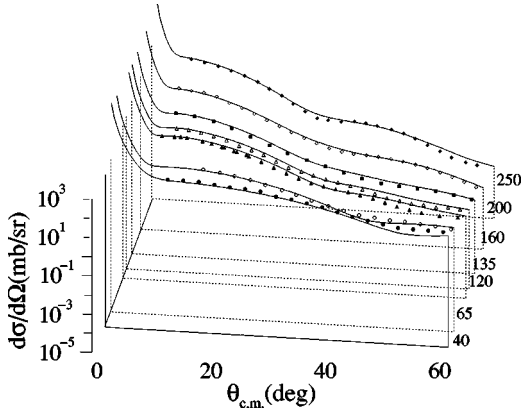

FIG. 1. Differential cross sections from the elastic scattering of 40 to 250 MeV protons from ^{12}C. The solid curves display our predictions obtained from single calculations with the complete nonlocal optical potentials formed by *g* folding.

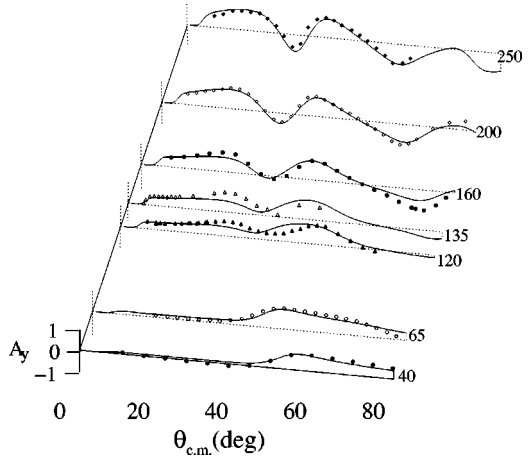

FIG. 3. As for Fig. 1, but for the analyzing powers from the elastic scattering of 40 to 250 MeV protons from ^{12}C.

proton-^{12}C optical potentials at each of the 18 values of energy we consider. At each energy we have used the OBDME specified by the $(0+2)\hbar\omega$ shell model wave function and bound states with which good electron scattering form factors were found. Thus there is no adjustable parameter considered with the use of DWBA98 in finding cross sections and analyzing powers. The solid curves in all figures shown in this section are the results of making a single calculation in each case. The results of calculations made with the full nonlocal *g*-folding optical potential we define for brevity hereafter as *complete*.

In Figs. 1 and 2 the results of our complete calculations of the differential cross sections from proton-^{12}C elastic scattering are compared with data. In Fig. 1 the results for 40 to 250 MeV are displayed while in Fig. 2 the higher energies from pion threshold are given. The individual energies are listed with each set and clearly the energy variation of the cross sections is reproduced quite well by our results. The associated analyzing powers are displayed in Figs. 3 and 4. In the first of those, with energies below pion threshold, the data and its energy trend are quite well fit by the results of our complete calculations. Some improvement is needed at energies near 135 MeV, but the overall pattern of the results is very good. For energies 300 MeV and higher, the trend of the analyzing power data again is reflected in the results of our calculations but there is some mismatch in the magnitude of the analyzing powers at forward angles and most evidently with 400 MeV.

Other spin observables have been measured at 65 and 500 MeV. Those data and our predictions are compared in Fig. 5 where the 65 MeV spin rotation $R(\theta)$ and the 500 MeV $D_{SS}(\theta)$ and $D_{SL}(\theta)$, are displayed in the top, middle, and bottom segments, respectively. Our predictions agree as well with these data as they do with the analyzing powers at each energy.

These plots suffice to give credence to the optical potentials formed by *g* folding at least as a good first order guess at the proton-^{12}C interaction. We consider each of the energy results in more detail now.

The DWBA98 code allows us to make calculations also with the integral term of the nonlocal Schrödinger equation omitted. This corresponds to ignoring the exchange effects

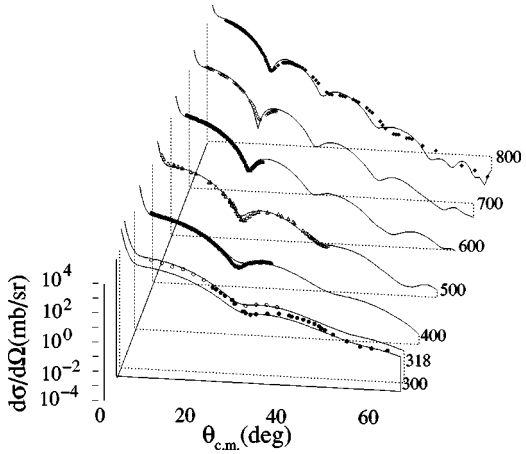

FIG. 2. As for Fig. 1 but for the elastic scattering of 300 to 800 MeV protons from ^{12}C.

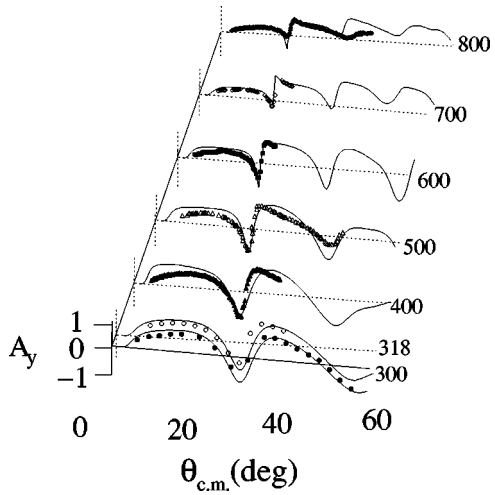

FIG. 4. As for Fig. 1 but for the analyzing powers from the elastic scattering of 300 to 800 MeV protons from ^{12}C.

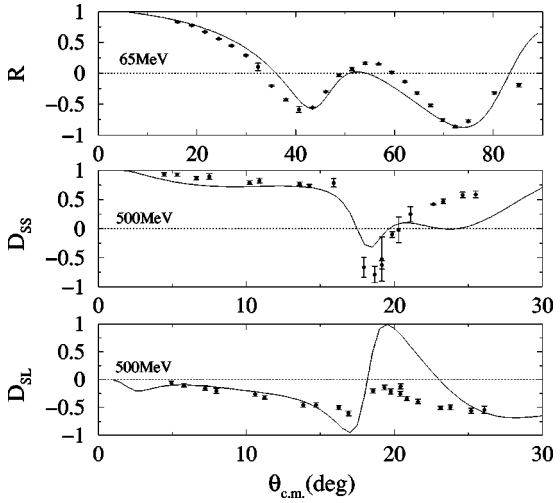

FIG. 5. The spin rotation $R(\theta)$ from the elastic scattering of 65 MeV protons from ^{12}C (top), and the observables, $D_{SS}(\theta)$ (middle), and $D_{SL}(\theta)$ (bottom) from the elastic scattering of 500 MeV protons from ^{12}C.

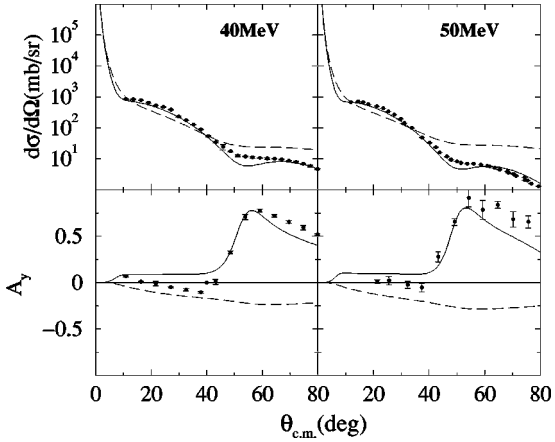

FIG. 6. Differential cross sections (top) and analyzing powers (bottom) from the elastic scattering of 40 and 50 MeV protons from ^{12}C. The solid curves display our predictions obtained from single calculations with the complete nonlocal optical potentials formed by g folding. The dashed curves are the results obtained when exchange effects are ignored therein. The data were taken from Refs. [8,9].

due to antisymmetrization of the $A+1$ scattering state. While that is a form of a $g\rho$ approximation, it is far more severe than any localization procedure of coordinate space optical potentials [6] or of the approximations leading to the $g\rho$ and $t\rho$ models in momentum space [3]. However, our purpose is not to find a best fit to data with the local term as that requires scaling and/or profile adjustment. Rather we make these approximate calculations to define just how large is the effect of the specific nonlocal component in the coordinate space optical potential. It is substantial as will be seen at most energies and so, in most cases, localization or any approximation for nonlocality must be recognized as a representation of a large effect. The results of omitting those exchange (knock-out) effects in the specification of the coordinate space optical potentials are displayed in the figures by the dashed curves and are defined hereafter as *no-exchange* results.

In the ensuing set of figures, for energies above pion threshold ($\sim$300 MeV) we present data and results to 40° scattering angle. There is little if any data at larger scattering angles. At lower energies we limit study to 80° as by then the data are so small in magnitude that calculated results may be overly sensitive to small changes in phase shifts.

The results of our calculations are compared with the 40 and 50 MeV data in Fig. 6. The complete results are in good agreement with data but those from the no-exchange calculations are not. The complete calculations give especially good results for the forward angle cross sections (to $\sim$40°). At the larger scattering angles the predictions have slightly more defined minima than evident with the data. The analyzing powers at these energies are shown in the bottom segments of Fig. 6, and while our complete calulations are quite reasonable in comparison with the data, there is room for improvement in those fits. That is the case for almost all of the energies studied and indicates that details of the scattering theory relating to the effective interactions currently used needs to be improved. Of course, as the analyzing powers are measures of differences between scattering probabilities and are normalized by the differential cross sections, predictions of analyzing powers are very sensitive to such details.

With both the cross sections and analyzing powers, however, it is clear that exchange effects cannot be ignored in making any analysis. The exchange amplitudes destructively interfere with the direct scattering amplitudes to markedly change the shapes of the predictions as well as to reduce considerably the size of the calculated cross sections at larger scattering angles.

The results found for 65 and 120 MeV proton scattering from ^{12}C are compared with the data in Fig. 7. Again only the results found using the complete calculations match observation. As with the lower energies, while those predicted cross sections are in good agreement with the data there are slight differences in structure to what is observed at the larger scattering angles. The analyzing powers again are reasonable results in comparison to the data although the 120

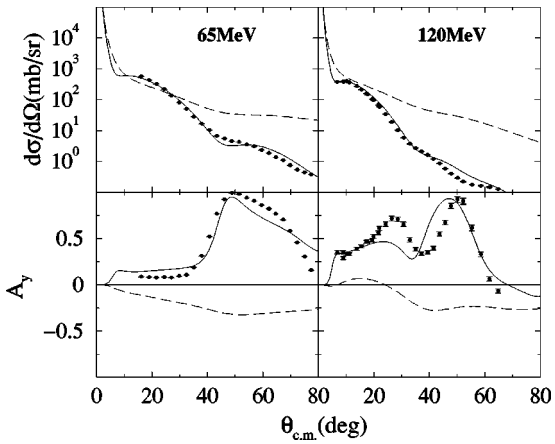

FIG. 7. As for Fig. 6 but for energies of 65 and 120 MeV. The data were taken from Refs. [10,11].

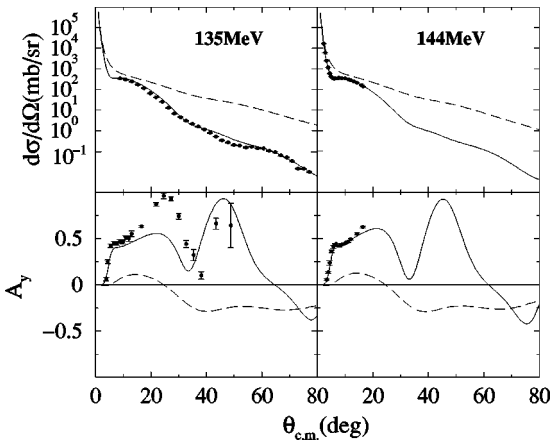

FIG. 8. As for Fig. 6 but for energies of 135 and 144 MeV. The data were taken from Refs. [12–14].

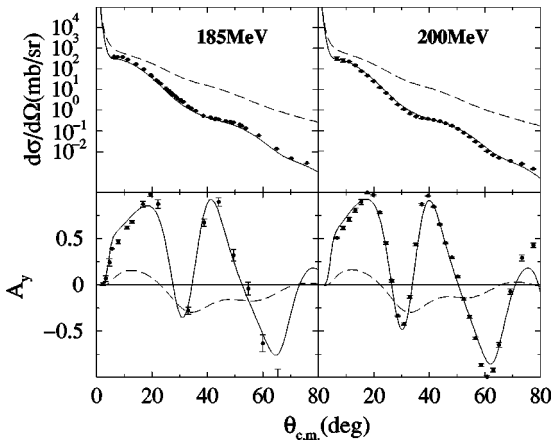

FIG. 10. As for Fig. 6 but for energies of 185 and 200 MeV. The data were taken from Refs. [17,18].

MeV predictions do not give the relative sizes or exact angle locations of the peak values in the data. However, compared with the results obtained with the no-exchange potentials, the complete calculations are excellent fits to data. The cross sections found using the no-exchange local potentials are much too large and have the wrong fall off with scattering angle in comparison with the data. The analyzing powers so calculated are completely at variance with observation.

In Fig. 8, results equivalent to those discussed above, are compared with the data taken with 135 and 144 MeV protons. Clearly the exchange amplitude contributions are extremely important. Without them the calculated cross sections become increasingly in disagreement with the measured data and by orders of magnitude with increasing scattering angle. Likewise the analyzing powers from the no-exchange local potential calculations are totally wrong. The complete calculations are in stark contrast giving as good replications of the cross section data as found at the lower energies discussed above, but the analyzing powers need improvement. The 135 MeV analyzing power result, similar to the 120 MeV case, does not agree with the structure seen in the data, notably being too small compared to the forward scattering positive peak value and not giving the correct angle values for the maxima. The data at 144 MeV are too limited in momentum transfer but one can suspect that new data would reflect what has been found at 135 MeV.

Our predictions of proton-^{12}C elastic scattering for 156 and 160 MeV, for 185 and 200 MeV, and for 250 and 300 MeV, are compared with the data in Figs. 9, 10, and 11, respectively. In all cases it is very evident that omission of the exchange amplitudes is a serious problem in analyses. The complete calculations give cross sections in very good agreement with the data, albeit that for 300 MeV the resultant fit is not as good as those at all lower energies. But it is with the analyzing powers that we note results that are better than we have found for the lower energies. With all six energies in these three figures, the locations of maxima in the observed analyzing powers, both positive and negative values, are correctly predicted. Also the magnitudes of the peaks in the analyzing powers are better reproduced, with the calculated value of the first positive peak increasing first to be almost complete asymmetry (1.0) and in agreement with the data at 200 MeV while slowly decreasing from that at the higher energies. In fact the data values of that peak decrease more rapidly than do the calculated values.

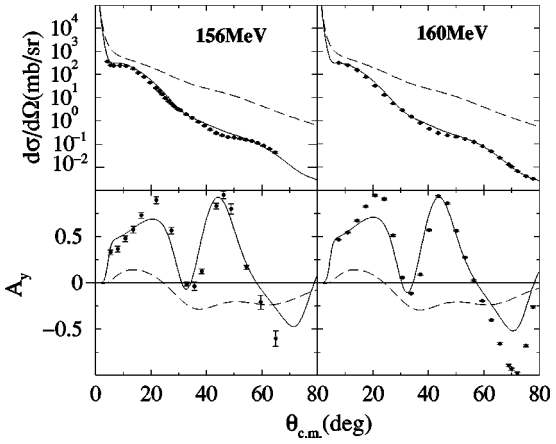

FIG. 9. As for Fig. 6 but for energies of 156 and 160 MeV. The data were taken from Refs. [15,16].

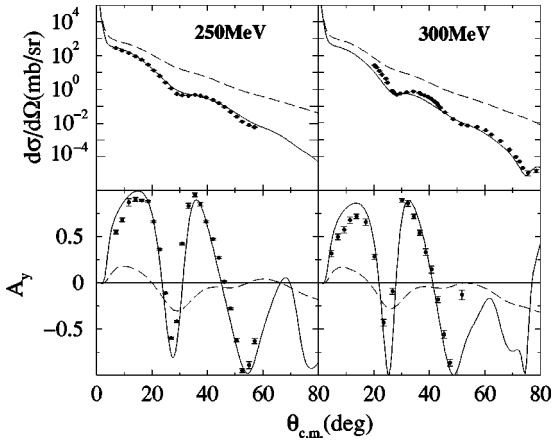

FIG. 11. As for Fig. 6 but for energies of 250 and 300 MeV. The data were taken from Refs. [19–21].

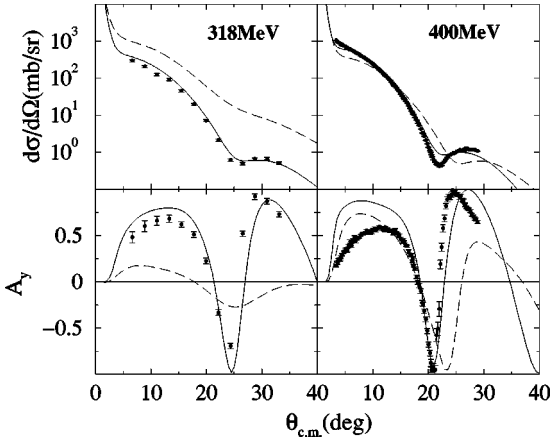

FIG. 12. As for Fig. 6 but for energies of 318 and 400 MeV. The data were taken from Refs. [22,23].

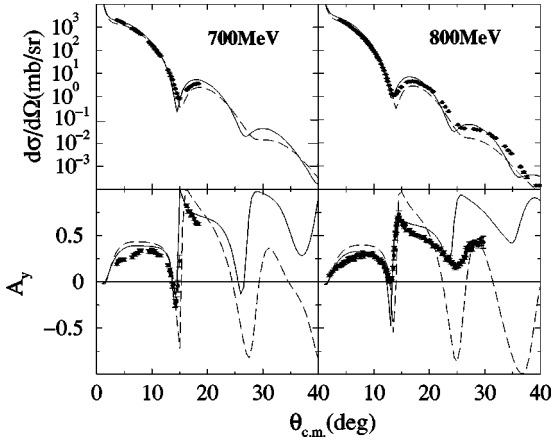

FIG. 14. As for Fig. 6 but for energies of 700 and 800 MeV. The data were taken from Refs. [23,25].

The results of our calculations for proton energies at and above pion threshold are shown in Figs. 12, 13, and 14 for the energy pairs 318 and 400 MeV, 500 and 600 MeV, and 700 and 800 MeV, respectively. In these cases, the effective *NN* interactions have been formed by supplementing the bare BCC3 interaction with complex short ranged Gaussian *NN* optical potentials with strengths set to ensure a match with the *NN* scattering phase shifts at each relevant energy. Again the results found by using the complete (g-folding) optical potentials and the no-exchange local ones are displayed by the solid and dashed curves in each figure. At 318 MeV, as is evident in Fig. 12, the complete calculation gives a very good fit to the cross section data and to the analyzing power data, save that the forward peak value is overpredicted. The no-exchange potential calculation results are at great odds with the data as they were at the lower energies. But at 400 MeV and higher, the influence of the exchange amplitudes diminishes in size and quite rapidly with energy. The complete and no-exchange calculation results still differ, however, with the results found with complete calculations giving better agreement with observation.

In Fig. 12, the results of our 400 MeV calculations are compared with the data taken at 398 MeV. Of all results these give the poorest fit to data. The complete calculation nevertheless gives a cross section that agrees with the data to about 20° scattering angle, but the sharp minima observed is not reproduced. Likewise the gross features of the 398 MeV analyzing power data are reproduced, but the forward peak is overpredicted.

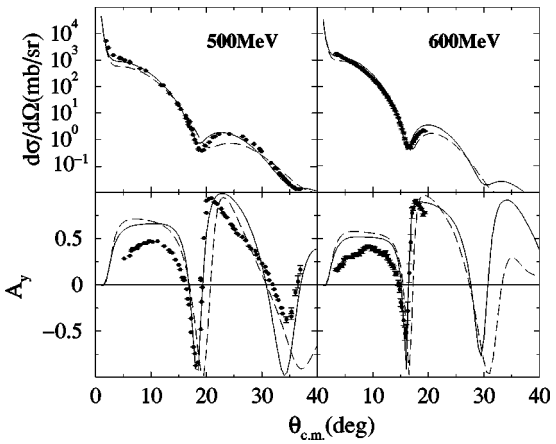

FIG. 13. As for Fig. 6 but for energies of 500 and 600 MeV. The data were taken from Refs. [23,24].

The results of 500 and 600 MeV calculations are compared with 500 and 597 MeV data in Fig. 13. While the results from the calculations made using the no-exchange local potentials are not greatly different from the complete calculation results now, the latter remain the better predictions of the actual data. The differential cross sections are very well reproduced with the sharp minima at about 20° being matched quite well. Likewise the predictions of the analyzing powers are fits to the data that improve upon the results found at 400 MeV. The forward peak in the analyzing power is still overpredicted but the trend with energy of that peak decreasing in size is found. The 500 MeV analyzing power results at scattering angles larger than $\sim 20°$ are not well reproduced, but this is where the cross section is small (order of a few tenths of a mb/sr) and so is sensitive to small details in the optical potential calculations.

Next, in Fig. 14, the complete and no-exchange local optical potential calculation results are compared with data for 700 and 800 MeV scattering. The cross sections are well fit by the results of the complete calculations with the no-exchange results being almost as good. The analyzing powers are reasonably well reproduced by both calculations with the calculated forward angle positive peak now in quite good agreement with the data. The analyzing power results are again in good agreement with data for those scattering angles at which the cross sections are larger than a few tenths of a mb/sr.

Other predictions of 800 MeV proton-^{12}C elastic scattering are compared with data in Fig. 15. The differential cross sections are given in the top segments while the analyzing powers are shown in the bottom segments of these figures. In the left hand side panels the data are compared with the results of our calculations made using the density-dependent effective interactions obtained from the g matrices associated with the bare OSBEP [32] and BCC3 [31] model potentials.

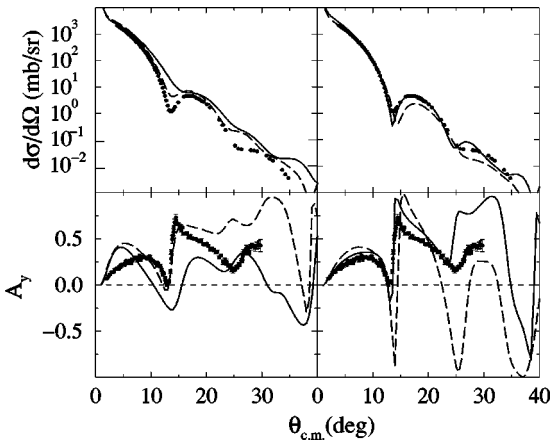

FIG. 15. Differential cross sections (top) and analyzing powers (bottom) for 800 MeV proton scattering from ^{12}C. In the left panel the data [25] are compared with predictions made using effective interactions based upon the bare OSBEP and BCC3 g matrices (solid and dashed curves). In the right panel the data are compared with predictions obtained from folding the modified OSBEP effective interactions. The solid curves portray our predictions with the complete optical potential. The dashed curves are the results when nonlocality is removed (the no-exchange approximation).

Those results are portrayed by the solid and dashed curves, respectively. In the right-hand side panels the same data are compared with our predictions determined from optical potentials defined by exclusion of any nonlocal elements (i.e., the $g\rho$ approximation) and by the complete (nonlocal) set of contributions. The solid and dashed curves in these cases depict the results we have found by using the modified OSBEP interaction in the complete and no-exchange calculations, respectively. Neither the OSBEP nor the BCC3 interactions fit well the observed on-shell *NN* data at 800 MeV. This is again evident from the comparisons given in left hand panel of Fig. 15 as neither lead to *pA* optical potentials, and thence scattering phase shifts from complete calculations, with which one can describe the observed proton-^{12}C data. The (complex) nature of the BCC3 interaction improves the situation in comparison to use of the purely real OSBEP force, but not sufficiently to explain the proton-^{12}C data. In rather stark contrast, using the *NN* interactions modified by *NN* optical potentials, we obtain proton-^{12}C optical potentials with which the cross section and analyzing power data are quite well reproduced. Most noticeable though is that the analyzing powers now are predicted well, and especially at forward scattering angles. The differential cross-section data of 800 MeV protons scattering from of ^{12}C have been very well reproduced to scattering angles of 25° by which the magnitudes have fallen to less than 0.1 mb/sr. The effects of the modulation of both the OSBEP and the BCC3 models are very noticeable. That is even more the case with the analyzing powers. Only with the modulations that tune OSBEP and BCC3 against the SM97 data set has satisfactory reproductions of that analyzing power structure been found. Specific medium effects in the effective *NN* interaction do not seem very important at 800 MeV, although such have been included in all of our analyses.

IV. CONCLUSIONS

Fully microscopic model calculations of coordinate space optical potentials describing proton-^{12}C elastic scattering at 18 energies in the range from 40 to 800 MeV have been made. Both differential cross section and analyzing power data have been analyzed at all energies considered. The complex optical potentials were formed by folding effective *NN* interactions with the density matrices of the ground state of ^{12}C. A complete $(0+2)\hbar\omega$ shell model calculation provided those density matrices. The effective interactions were obtained by mapping half-off-shell *NN* g matrices (solutions of BBG equations) associated with Bonn potentials supplemented above pion threshold by short ranged Gaussian *NN* optical potentials so that all *NN* scattering phase shifts to over 1 GeV were reproduced. The results of the g-folding process are complex, nonlocal proton-^{12}C potentials. Solution of the integrodifferential Schrödinger equations formed with those optical potentials resulted in good to excellent fits to elastic scattering data at all energies, both the cross sections and the analyzing powers.

Our results confirm the large effect of the (knock-out) exchange amplitude in the elastic scattering process and which make the coordinate space optical potentials nonlocal. This is of import at all energies save for perhaps the highest. In almost all past coordinate space studies of p-A elastic scattering, be they with a Schrödinger, Dirac, or relativistic impulse approximation formulation, inherent exchange amplitudes either have been ignored or localized.

Although our predictions of the scattering are good at all energies they are better for energies below pion threshold than above. Notably at energies above pion threshold, our best results for the forward scattering angle analyzing powers overpredict the data. This may be due to the treatment of pion production and resonance effects being too simplistic and not providing pertinent off-shell properties of the *NN* t, and g matrices at those energies to specify the appropriate details the effective interactions.

ACKNOWLEDGMENTS

We acknowledge the financial support of the Australian Research Council (ARC) given to pursue this research.

[1] L. Allen, K. Amos, and P. J. Dortmans, Phys. Rev. C **49**, 2177 (1994), and references cited therein.

[2] P. E. Hodgson, *The Nucleon Optical Model* (World Scientific, Singapore, 1994); S. G. Cooper and R. S. Mackintosh, Phys. Rev. C **54**, 3133 (1996).

[3] H. F. Arellano, F. A. Brieva, M. Sander, and H. V. von Geramb, Phys. Rev. C **54**, 2570 (1996); Ch. Elster, S. P. Weppner, and C. R. Chinn, *ibid.* **56**, 2080 (1997), and references cited

therein.
[4] S. Karataglidis, P. J. Dortmans, K. Amos, and R. de Swiniarski, Phys. Rev. C **52**, 861 (1995); **52**, 3224 (1995).
[5] P. J. Dortmans, K. Amos, and S. Karataglidis, J. Phys. G **23**, 183 (1997); P. J. Dortmans, K. Amos, S. Karataglidis, and J. Raynal, Phys. Rev. C **58**, 2249 (1998).
[6] K. Amos, P. J. Dortmans, H. V. von Geramb, S. Karataglidis, and J. Raynal, Adv. Nucl. Phys. (in press).
[7] J. J. Kelly and S. J. Wallace, Phys. Rev. C **49**, 1315 (1994), and references cited therein.
[8] L. N. Blumberg, E. E. Gross, A. van der Woude, A. Zucker, and R. H. Bassel, Phys. Rev. **147**, 812 (1966).
[9] J. A. Fannon, E. J. Burge, D. A. Smith, and N. K. Ganguly, Nucl. Phys. **A97**, 263 (1967).
[10] S. Kato *et al.*, Phys. Rev. C **31**, 1616 (1985).
[11] J. R. Comfort *et al.*, Phys. Rev. C **24**, 1834 (1981).
[12] W. Bauhoff *et al.*, Nucl. Phys. **A410**, 180 (1983).
[13] J. M. Dickson and D. C. Salter, Nuovo Cimento **6**, 235 (1957).
[14] O. N. Jarvis, C. Whitehead, and M. Shah, Nucl. Phys. **A184**, 615 (1972).
[15] V. Comparat, Ph.D. thesis, Centre d'Orsay, Université Paris-Sud, 1975.
[16] H. O. Meyer, P. Schwandt, W. W. Jacobs, and J. R. Hall, Phys. Rev. C **27**, 459 (1983).
[17] A. Ingermarsson, O. Jonsson, and A. Hallgren, Nucl. Phys. **A319**, 377 (1979).
[18] J. R. Comfort, G. L. Moake, C. C. Foster, P. Schwandt, and W. G. Love, Phys. Rev. C **26**, 1800 (1982).
[19] H. Takeda *et al.*, RCNP annual report, 1995 (unpublished), p. 1.
[20] H. O. Meyer *et al.*, Phys. Rev. C **31**, 1569 (1985).
[21] H. Sakaguchi *et al.*, RCNP annual report, 1993 (unpublished), p. 4.
[22] F. T. Baker *et al.*, Phys. Rev. C **48**, 1106 (1993).
[23] K. W. Jones *et al.*, Phys. Rev. C **50**, 1982 (1994); Phys. Lett. **128B**, 281 (1983); Phys. Rev. C **33**, 17 (1986).
[24] G. W. Hoffmann *et al.*, Phys. Rev. C **41**, 1651 (1990).
[25] G. S. Blanpied, C. Shekhar Mishra, and B. G. Ritchie, Phys. Rev. C **33**, 1527 (1986).
[26] J. Raynal, Report No. NEA 1209/02, 1981 (unpublished); K. Amos, University of Melbourne Report No. UM-P-98, 1998 (unpublished).
[27] L. Rikus, K. Nakano, and H. V. von Geramb, Nucl. Phys. **A414**, 413 (1984); L. Rikus and H. V. von Geramb, *ibid.* **A426**, 496 (1984).
[28] S. Cohen and D. Kurath, Nucl. Phys. **73**, 1 (1965); D. J. Millener and D. Kurath, Nucl. Phys. **A255**, 315 (1975).
[29] S. Karataglidis, P. J. Dortmans, K. Amos, and R. de Swiniarski, Aust. J. Phys. **54**, 644 (1996).
[30] H. V. von Geramb, K. Amos, L. Berge, S. Bräutigam, H. Kohlhoff, and A. Ingermarsson, Phys. Rev. C **44**, 73 (1991); P. J. Dortmans and K. Amos, *ibid.* **49**, 1309 (1994).
[31] R. Machleidt, Adv. Nucl. Phys. **19**, 189 (1989); R. Machleidt, K. Holinde, and Ch. Elster, Phys. Rep. **149**, 1 (1987); R. Machleidt and G.Q. Li, *ibid.* **242**, 5 (1994).
[32] L. Jäde and H. V. von Geramb, Phys. Rev. C **57**, 496 (1998); L. Jäde, *ibid.* **58**, 96 (1998).
[33] Ch. Elster, W. Ferchländer, K. Holinde, D. Schütte, and R. Machleidt, Phys. Rev. C **37**, 1647 (1988); A. Bulla and P.U. Sauer, Few-Body Syst. **12**, 141 (1992), and references cited therein.
[34] H. V. von Geramb, K. Amos, H. Labes, and M. Sander, Phys. Rev. C **58**, 1948 (1998).
[35] R. A. Arndt, C. H. Oh, I. I. Strakovsky, R. L. Workman, and F. Dohrmann, Phys. Rev. C **56**, 3005 (1997).
[36] L. Ray, Phys. Rev. C **41**, 2816 (1990).